RESEARCH PAPER

Effect of Strain Induced Martensite on the Deep Drawing Behavior of 304L Steel: Simulation and Experiment

H. Fathi[1], B. Mohammad Sadeghi[2,*], E. Emadoddin[1] and H. R. Mohammadian Semnani[1]

**bmsadeghi@iust.ac.ir*

Received: May 2018 **Revised: January 2019** **Accepted: April 2019**

[1] Faculty of Materials and Metallurgical Engineering, Semnan University, Semnan, Iran.

[2] School of Metallurgy and Materials Engineering, Iran University of Science and Technology, Tehran, Iran.

DOI: 10.22068/ijmse.16.2.33

Abstract: *In the present research, the behavior of 304L austenitic stainless steel in the deep drawing process has been studied at the room temperature through experimental and finite element simulation method. Magnetic method calibrated by XRD was used to measure induced-martensite. Martensite volume fraction in the various portion of the deep-drawn cup under optimum blank holder force (BHF) and in the rupture location was evaluated. Findings of the present study indicated that higher martensite volume fraction occurred in the flange portion in the drawn cup due to higher strain and stress concentration in this area. Also, rupture happened at the arc portion of the wall of drawn cup with higher blank diameter due to higher strain, work hardening, and martensitic transformation. Both experimental and simulation results showed that maximum LDR of 2 obtained in the forming process. All experimental procedures were simulated by LS-DYNA software, employing MAT_TRIP, and experimental results were in good agreement with the FE simulation.*

Keywords: *Stress; Strain; Triaxiality; Martensitic transformation; Austenitic stainless steel; Deep drawing*

1. INTRODUCTION

In recent years, using stainless steel as a structure with high fracture resistance is considered because of the high energy absorption and good formability. Stainless steels are useful and suitable for engineering applications in major industries such as chemistry, automotive, aerospace, and submarine. Martensitic transformation is a well-known phenomenon that occurs in austenitic stainless steel 304L. Indeed, heat treatment process does not affect the mechanical properties of austenitic stainless steels such as yield strength, ductility, and formability of this material, while the mechanical properties change with strain hardening process [1-5]. Both ductility and strength may be enhanced in austenitic stainless steels by the generation of martensite through phase transformation phenomenon [6].

Since the metallic material with the shape of blank is very used in the various industries such as the automotive and aerospace industries; therefore, recognition and understanding the process of the sheet metal forming has been considered [7, 8]. Deep drawing is a simple and important process which is used to produce the complex parts from sheet metals in large volume such as flashlight body, aluminum, and steel canister. More geometrical and physical parameters such as die and punch diameter, punch speed, temperature, friction coefficient, lubricant, distance between punch and die, BHF and type of material on achieving products without any problems are effective in the deep drawing process. It should be noted that considering all parameters to obtain a product with high quality is necessary [9-13]. The main problems occurring during deep drawing process are tearing and fracture, wrinkling (the most important problem), necking and drawing grooves [14-16]. In addition, there is a main challenge in sheet metal forming process that geometric distortion of the sheet metal emerges after forming process, which is known as the spring back [17]. In the deep drawing process, BHF affects the wrinkling and tearing of the sheet. Blank holder prevents wrinkling and movement of the sheet when the sheet is driven into the die. Therefore, the optimal value for the BHF must be determined in order to achieve the formed sheet without any tearing and wrinkling during forming [18-20].

It is proven that strain rate, stress state, strain, temperature, stacking fault energy (SFE), and triaxiality factor affect the behavior and formability of austenitic stainless steels [21-23]. Since strain-induced martensite volume fraction relates directly to the amount of strain, therefore more induced martensite transforms in the lo-

[DOI: 10.22068/ijmse.16.3.32]

Table 1. Chemical composition of the initial material (wt%).

Fe	C	Si	Mn	S	P	Cr	Ni	Co	V	Remain
Base	0.026	0.55	1.07	0.001	0.029	18.38	8.18	0.37	0.112	Other elements

cation with high strain. For these reasons, recognition, and analysis of stress and strain in various region of the drawn cup are very important in order to control the forming process and obtain a final product without any defects. Therefore, the state of stress and state of strain should be determined for various regions of the cup such as the wall, bottom, and flange of the cup. Stress and strain state in the deep-drawn cup with maximum limit drawing ratio (LDR) under optimum BHF and strain rate were determined and volume fraction of induced martensite (VFM) has been related to them.

Nowadays, numerical analysis is used for prediction and designation of the metal forming process due to the vital role in some industries such as automotive and aerospace. For this reason, finite element (FE) method is replacing the experimental procedures to predict the behavior of the material during the process. Numerical simulation in metal forming can be useful to obtain optimized parameters in some technological problems such as wrinkling, necking, and fracture [14, 17, 18, 24]. In this paper, finite element method using Trip material model (MAT_TRIP) in LS-DYNA software was used to predict martensite volume fraction, strain and stress state for validating the experimental results.

2. MATERIALS AND METHODS

2.1. Experiments

A fully austenitic stainless steel sheet with a thickness of 0.5 mm was provided as the initial material for experimental test. Chemical composition of the initial material, shown in Table 1, reveals that the material is an austenitic stainless steel type 304L. Circular blanks with diameter vary from 78 to 90 mm with an increment of 2 mm were provided to perform deep drawing tests and determine the optimum parameters such as BHF and maximum LDR. Circular grid pattern with 2.5 mm diameter was chemically etched on the surfaces of the blanks to measure strains at various locations of the cup after drawing process.

Teflon sheet was used between blanks and die in order to reduce friction and minimizing the shear stress in sheet at the contact interface. The friction coefficient is set to low in order to allow the material to control the forming process [12]. In this study, a set of die and punch with a diameter of 41.5 and 40 mm, respectively, used to perform deep drawing tests using a 40-ton hydraulic press equipped by a computer, as shown in Fig. 1(a) and Fig. 1(b).

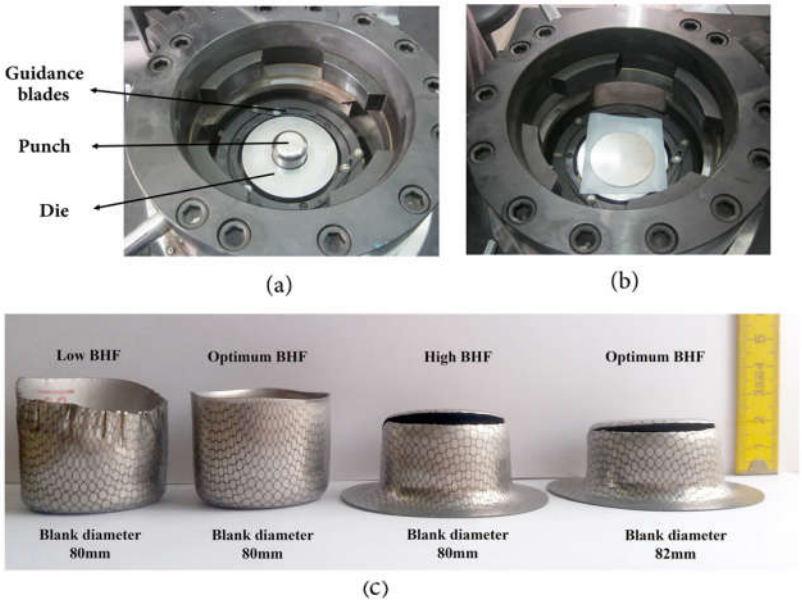

Fig. 1. (a): set of die and punch; (b): placement of blank and Teflon on the die and (c): Deep drawn cups under various conditions

[DOI: 10.22068/ijmse.16.3.32]

Three guidance blades in die guided blank and located them at the center of the punch and die. It is pointed that increasing die radius leads to increase draw-ability and LDR, while higher die radius causes other problems and defects such as wrinkling of blank at the flange. For these reasons, the optimum radius of 8 mm was applied in the die [25].

Fig. 1(c) shows the deep-drawn cup from blank with a diameter of 80 mm under optimum (1600 kgf), low (1500 kgf), and high (1700 kgf) blank holder forces. Punch speed of 3 mm min^{-1}, low strain rate, was applied to obtained higher formability of the material [22]. Higher punch speed of 30 mm min^{-1} was used to study the deep draw-ability of the material under a higher strain rate.

Since, α'-martensite is a ferromagnetic phase, which is transformed from non-magnetic austenite phase in austenitic stainless steel [26], therefore magnetic saturation is a useful method to measure the induced martensite volume fraction. Based on the previous work, the magnetic saturation method was used to measure the volume fractions of martensite in different regions of the drawn cup such as flange, close to the flange, and wall [27]. In this case, the magnetic method was calibrated by XRD to evaluate the amount of martensite [27, 28].

Microstructures of the edge, wall, bottom of the cup, and near the rupture region were observed after etching using an optical microscope. Etchant was prepared from two solutions: first solution contained 0.3 g sodium metabisulfite in 50 mL distilled water and the second one contained 10 mL hydrochloric acid in 50 mL distilled water. The samples were immersed for 40 seconds in the etching solution.

2.2. Simulation

Simulation carried out with LS-DYNA using TRIP material (MAT113) to validate experimental results. Induced martensite volume fraction rate is determined by Eq. 1 in this material model [29]. Yield stress increases with the increase of strain rate but strain rate does not affect the ultimate tensile stress of austenitic stainless steel [22, 30, 31]. Therefore, yield stress may be changed during the deformation of the sheet under various strain rates. For this reason, MAT_TRIP calculates the yield stress of the material during the forming process through Eq. 2 and takes into account the Eq. 1 for calculating the rate of VFM [29].

$$\partial V_m/\partial \bar{\varepsilon}^p=\{(B/A)\exp\left(\frac{Q}{T-T_{A0}}\right)\left(\frac{1-V_m}{V_m}\right)^{(B+1)B} V \quad V_m{}^P \left(\frac{1}{2}\right)(1-\tanh(C+DT))\} \qquad \text{Eq.1}$$

$$\sigma_y=\{B_{Hs}-(B_{HS}-A_{HS})\exp(-m[\bar{\varepsilon}^p+\varepsilon_0]^n)\} \quad (K_1+K_2T)+\Delta H_{\gamma\rightarrow\acute{\alpha}}Vm \qquad \text{Eq.2}$$

where:

$\bar{\varepsilon}^p$: Effective plastic strain
Q: Heat capacity
T: Initial temperature
A,B,C,D,P,K1,K2,m,n,$\Delta H_{\gamma\rightarrow\acute{\alpha}}$: Martensite rate equation parameters
V_m: Initial volume fraction of martensite
ε_0: Pre-strain
A_{HS}, B_{HS}: Hardening law parameters

In this study, 3D modeling of the problem was applied in order to understand the real conditions of deformation during the deep drawing process. Fig. 2 shows 3D-modeling of the deep drawing process for determining VFM in all regions of the cup under optimum BHF and maximum LDR.

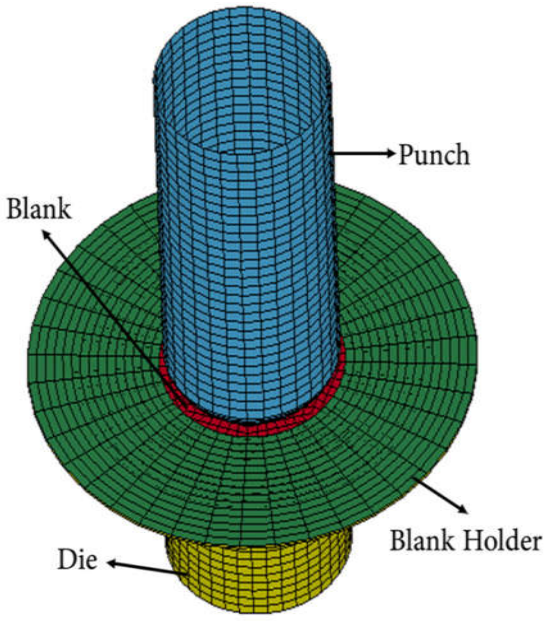

Fig. 2. 3D-modeling of the deep drawing process

[DOI: 10.22068/ijmse.16.3.32]

Various BHFs were simulated to obtain the optimum BHF and the effect of the BHF on the draw-ability of the sheet. After that, the result of the simulation method was validated with the experimental procedure.

3. RESULTS AND DISCUSSION

In the metal forming process, it is very important to recognize parameters that affect the process obtaining a final product without any defects. One of the key factors is stress state that should be known for designing the process of forming. Various stress states are imposed during the deep drawing of the sheet. For instance, traction equibiaxial stress state at the bottom, traction plane stress at the wall, traction-compression at the flange, and compression at the edge of the cup are existed [32]. Stress state conditions with stress tensors at different portions of the drawn cup are shown in Fig. 3.

Fig. 4 shows force-displacement curves of deep drawing process under optimum (1600 kgf), low (1500 kgf) and high (1700 kgf) blank holder forces. As can be seen, the load curve for high BHF is higher than the two others while punch load curve for low BHF is upper than optimum BHF. According to this figure, blank flaws into the die with maximum punch forces of 40000, 46000 and 50000 N at a displacement of 22 mm

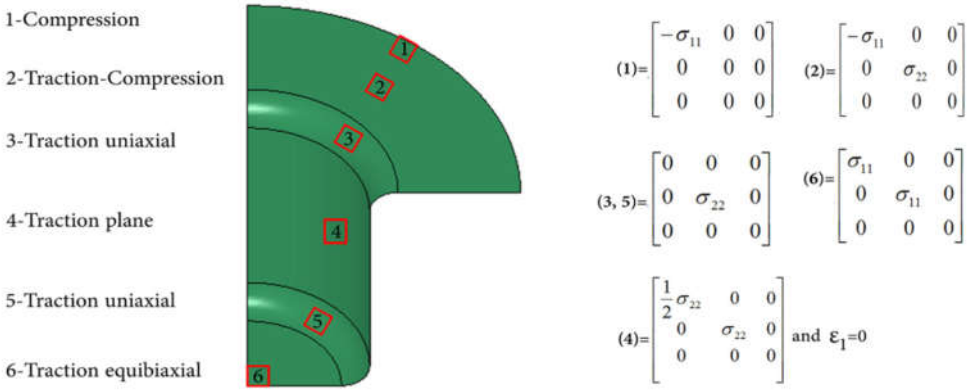

Fig. 3. Stress state condition at various regions of the drawn cup

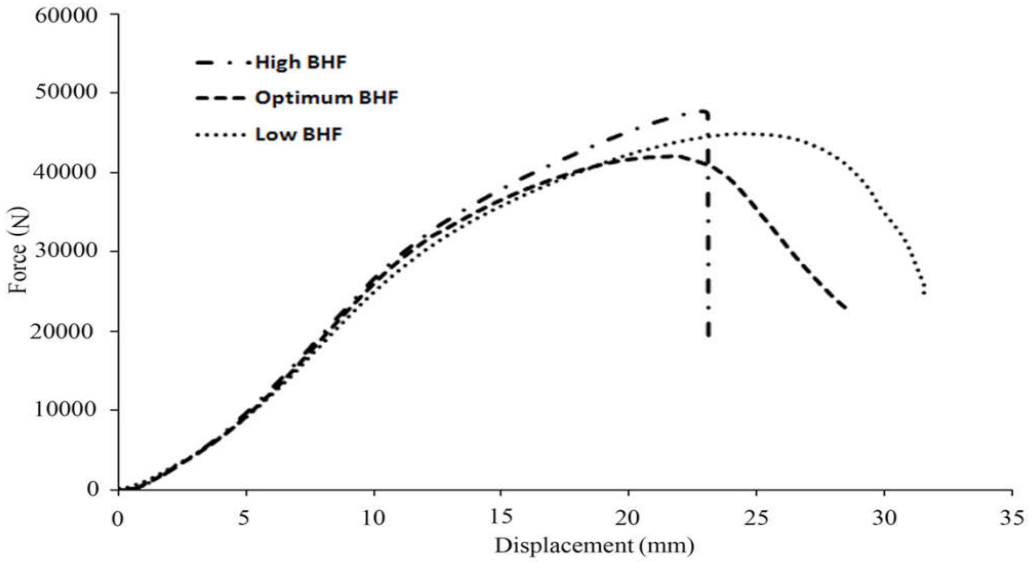

Fig. 4. Force-displacement curve under optimum, low, and high BHF

[DOI: 10.22068/ijmse.16.3.32]

under optimum, low, and high BHF, respectively. Applied punch force increases when blank starts going into the die until 40000 N at 22 mm, then material flow leads to the reduction in punch force. There is a similar case for the material flow with low BHF. In this case, material flows into the die and wrinkles occur on the edge of the circular blank due to insufficient force to hold the material between the die and blank holder, therefore material needs more punch force to flow into the die. For this reason, the force required to flow the material into the die with low BHF is increased to 46000 N. Considering this figure, different case exists for material flow with high BHF. The material can easily flow into the die while punch force increases during material's flow. High BHF prevents material flow leading to increase punch force up to 50000 N with a failure at the end wall of the cup (arc portion of the wall).

Fig. 5 illustrates the experimental and simulation results of the drawn cup under different conditions of blank holder forces. As can be seen, more stress concentration occurs in the flange with optimum and low BHF, while it occurs in the arc portion of the wall with high BHF. This is because the perimeter of the circular blank that

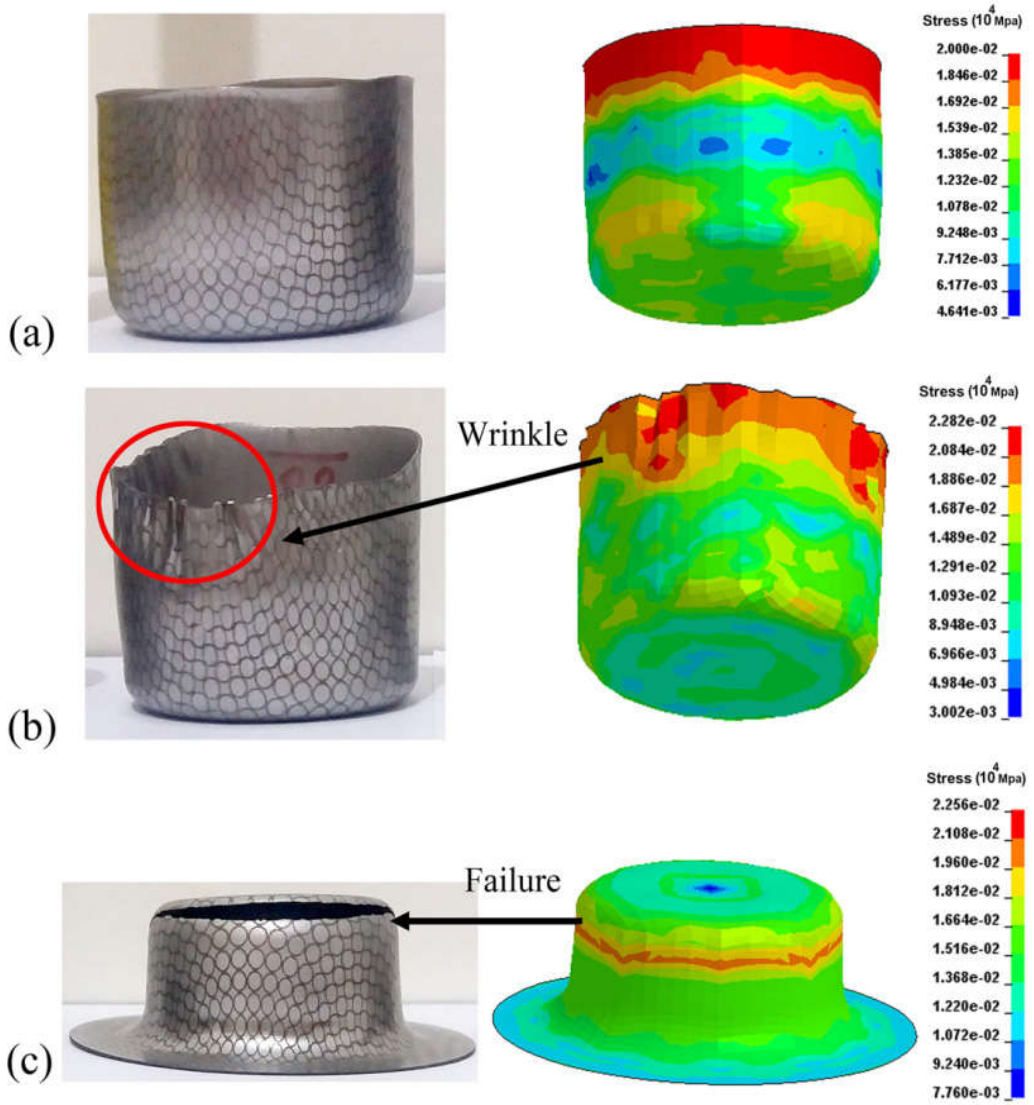

Fig. 5. Stress concentration, wrinkle and failure area of the drawn cup from a blank diameter of 80 mm under (a) optimum, (b) low and (c) high blank holder forces condition

[DOI: 10.22068/ijmse.16.3.32]

creates flange is under plastic deformation from beginning to the end of the forming process. Since circular blank edge goes into the die from the outer perimeter during the deep drawing process and it is severe in the final step that flange flows into the die, thus greater volume of material flows in the final step of drawing, therefore more strain occurs in the flange. It has been proven that increasing the compressive hoop stress in the flange portion leads to wrinkle in this region during deep drawing of the metallic sheet [16]. According to Fig. 5(b), wrinkles occur in the deep drawn cup under low BHF (1500 kgf) due to the increase in the compressive hoop stress in the flange, while higher BHF (1600 kgf) compensates the effect of the hoop stress in the flange and prevents the wrinkling in this area.

Limiting draw ratio (LDR) in the deep drawing of sheet metals is determined by Eq. 3.

$$LDR=D_{Max}/D_{Punch} \quad \text{Eq.3}$$

where DMax is the maximum blank diameter which is successfully drawn to a cup with an inner diameter of DPunch, punch diameter. In the present study, circular blank with a diameter of 80 mm was drawn without any defects, therefore maximum LDR of 2 was achieved.

Fig. 6 shows the thickness distribution of the drawn cup from a blank diameter of 82 mm and 80 mm in FE simulation being compared with experimental results. As can be seen in Fig. 6(a), circular blank with a diameter of 82 mm under optimum BHF was not completely drawn and experimental procedure confirmed FE simulation. Rupture occurs with increasing the blank diameter due to compressive hoop stress in the flange leading to an increase in the blank thickness of the flange during deep drawing. This figure illustrates that higher thickness happens in the flange portion, while lower thickness occurs in the cup bottom. When the punch begins to move, material flows into the die from the center to the outer diameter of the blank, where material moves from the perimeter of the blank, leading to an increase in the thickness of the blank in the flange portions. Increasing the thickness of the flange portion prevents the material flow into the die. Also, compressive hoop stress at the flange in radial direction increases the thickness of the flange [12, 33]. Cup wall plays an important role during the forming process and it transforms applied load to the cup bottom, therefore the thick-

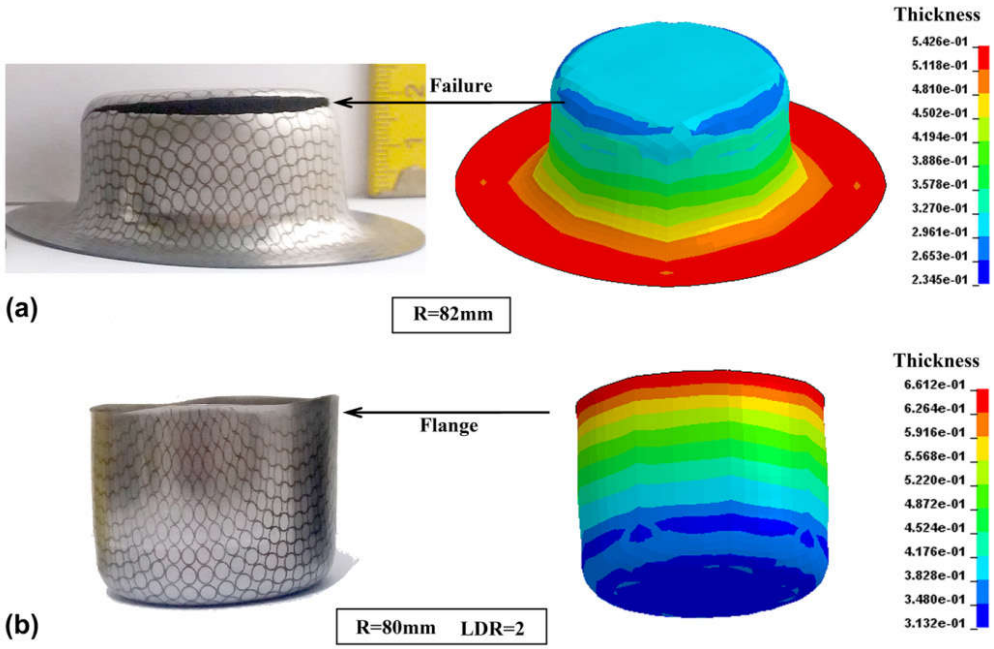

Fig. 6. Rupture loci and thickness distribution based on FE simulation in the deep drawn cup from circular blanks diameter of (a) 82 mm and (b) 80 mm under optimum conditio

[DOI: 10.22068/ijmse.16.3.32]

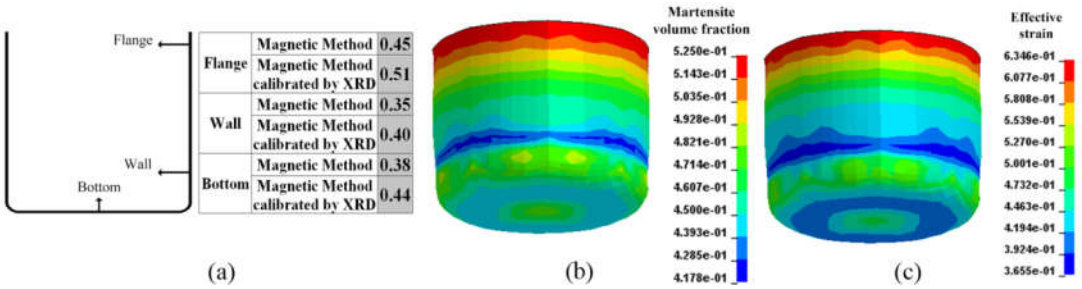

Fig. 7. Induced martensite distribution in
(a) experimental procedure, (b) FE simulation, and (c) distribution of effective strain

ness of the wall in the arc reduces enhancing the rupturein the arc portion of the wall. According to Fig. 6(b), thickness increases from the cup bottom to the flange portion in the deep-drawn cup under the optimum condition with LDR of 2.

Fig. 7(a) and Fig. 7(b) depict martensite volume fraction for various locations, i.e., flange, wall, and bottom of the drawn cup through the experimental procedure and FE simulation, respectively, while Fig. 7(c) shows the strain distribution for the deep-drawn cup without any defects under optimum condition. Both magnetic method and FE simulation output (see Fig. 7) show that more martensite transforms in the flange portion, while less martensite transforms in the wall of the cup. It should be mentioned that the volume fraction of induced-martensite is directly related to the strain, thus more martensite is transformed in the region with higher strain [27]. Experimental measurement of effective strain using Mylar transparent tape, Table 2, shows that maximum and minimum strain occurs in the flange portion and cup wall, respectively. Fig. 7(c) illustrates that higher strain occurs in the flange portion, however, lower strain happens in the wall of the cup.

Figs. 8(a), (b) and (c) show microstructure of the edge, wall, and bottom of the drawn cup under optimum condition, respectively. This figure shows that microstructure of the edge, wall, and bottom portion contain about 48.8%, 40.29%, and 45.86% martensite phase, respectively. These results indicate that experimental output data is carefully in agreement with FE simulation. Considering the Fig. 3, the flange and arc portion are under compression and traction state of stress in the deep drawing process. The flange is under compression at the initial stage and this phenomenon leads to an increase in the thickness of the flange. Also, this region is under tension in the final stage of the forming leading to form the final shape of the drawn cup. In this case, high strain occurs in the flange portion. Since martensitic transformation is as a function of strain, therefore higher volume fraction of martensite transforms in the flange portion.

It has been reported that biaxial tension condition intensifies martensitic transformation more than uniaxial tension, compression, and torsion condition on equal strains [34-36]. Stress triaxiality and strain have a combined effect on the transformation. Triaxiality factor is defined as $\Sigma=\sigma_m/\sigma_{equ}$ (where $\sigma_m=(\sigma_1+\sigma_2+\sigma_3/3$ and σ_{equ}= Equivalent von Mises stress). It is pointed out that probability of martensite nucleation at the

Table 2. Experimental and FE simulation outputs for martensite volume fraction and amount of strain at different location of the deep-drawn cup under optimum BHF.

	Strain		Martensite volume fraction		
	Experiment	Simulation	Experiment	Metallographic observation	Simulation
Flange	0.58	0.58-0.63	0.51	0.488	0.50-0.525
Wall	0.33	0.36-0.39	0.40	0.4029	0.41-0.43
Bottom	0.462	0.446-0.5	0.44	0.4586	0.45-0.48

[DOI: 10.22068/ijmse.16.3.32]

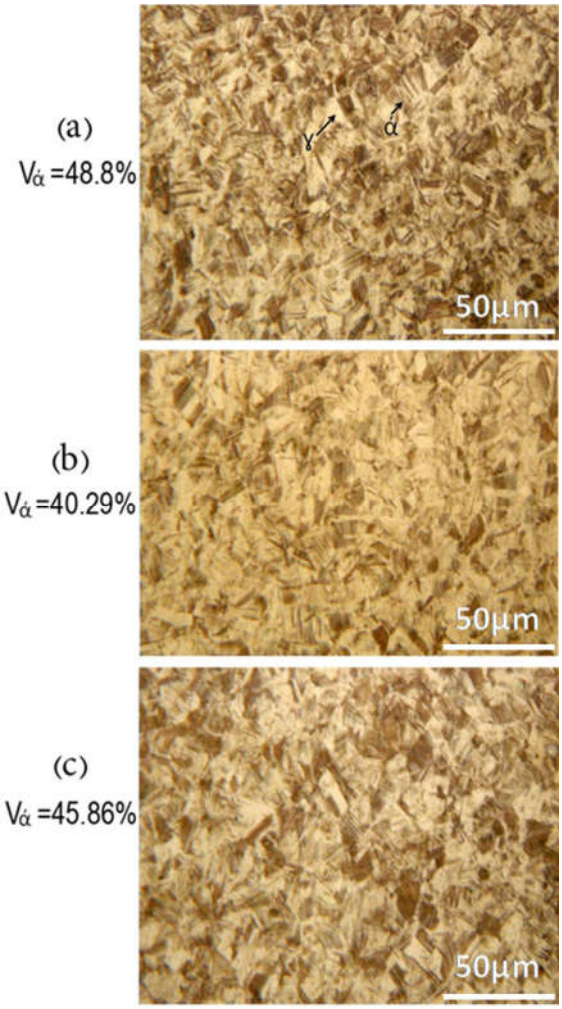

Fig. 8. Microstructure of the (a) edge, (b) wall, and (c) bottom of the drawn cup under optimum condition

potential sites enhances with increasing the triaxiality. Increasing triaxiality leads to enhancement of the thermodynamic driving force for martensitic transformation, therefore higher martensite volume fraction may be obtained [36].

In the case of stress sates with respect to the Fig. 3, triaxiality for various portions of the cup such as the 1, 3, 4, 5, 6 regions are as follows:

Region 1 (compression) → Σ= - 0.333
Region 3, 5 (Traction uniaxial) → Σ= 0.333
Region 4 (Traction plane) → Σ= 0.577
Region 6 (Traction equibiaxial) → Σ= 0.666

Martensitic transformation is a function of strain, therefore the highest strain at the flange causes the highest martensite volume fraction that was discussed earlier. Since the arc portion of the cup is under traction uniaxial stress state and triaxiality of this portion is equal to 0.333, which is the lower amount; therefore the least amount of martensite volume fraction is transformed in this region. Thickness reduction of the bottom causes increasing effective strain in this region. For these reasons, higher effective strain occurs at the cup bottom than the wall. Triaxiality of the wall and bottom of the cup are 0.577 and 0.666, respectively. In this case, higher strain and triaxiality are dominant at the bottom of the cup compared to the cup wall. As a result, higher martensitic transformation takes place in the bottom portion rather than cup wall, hence higher martensite volume fraction transforms in the bottom than cup wall. These results are summarized in Table 2 through experimental measurements and FE simulation.

According to experimental and FE simulation results, circular blank with a diameter of 82 mm was not successfully deep-drawn, Fig. 9. Martensite volume fraction was measured through experimental and simulation method, Figs. 9(a) and (b). In this case, induced martensite was evaluated using magnetic saturation and magnetic calibrated by XRD method and then validated by FE simulation. High strain hardening occurs with increasing the strain in austenitic stainless steel due to martensitic transformation and increase in martensite volume fraction enhancing elongation in this type of material [22, 37]. Metallographic observation (Fig. 9(c)) shows that microstructure of the fracture region contains about 58.23% martensite phase. Higher stress concentrates in the arc portion of the wall causes a rupture in this region. Considering Fig. 6(a) and Fig. 9(d), higher strain and lower thickness occur in the arc portion. Higher strain hardening happens when the material goes into the die and more elongation occurs in the material and this phenomenon leads to get high formability. During the forming process, the thickness of the flange increases due to compressive hoop stress preventing the material flow into the die, therefore elongation in the wall portion increases. In this case,

[DOI: 10.22068/ijmse.16.3.32]

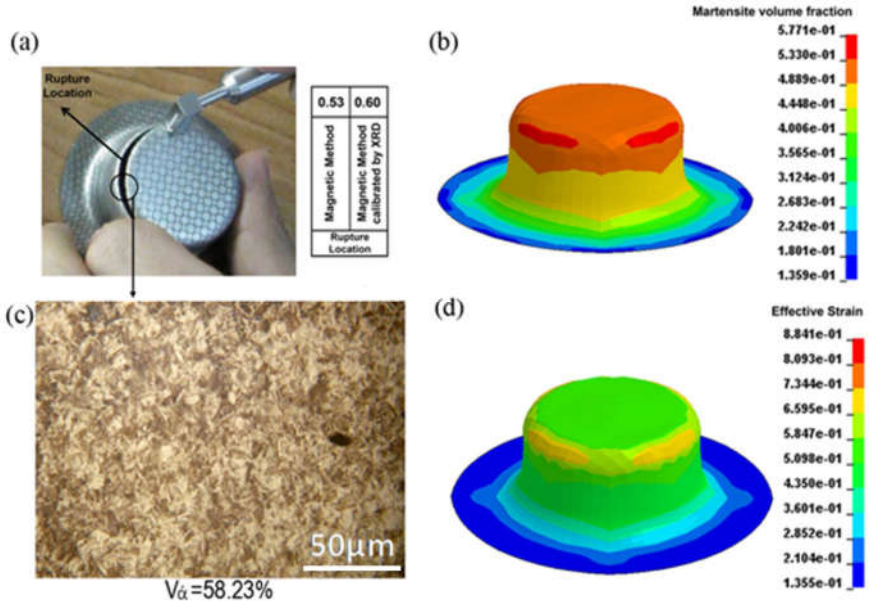

Fig. 9. Martensite volume fraction in the rupture loci for deep drawing of a blank with a diameter of 82 mm through (a) experimental, and (b) FE simulation; (c) microstructure of the fracture region, and (d) effective strain

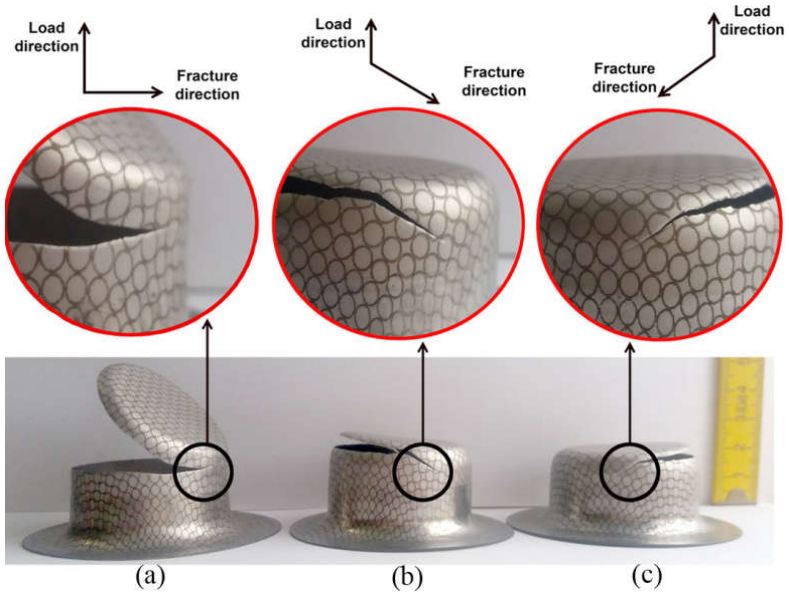

Fig. 10. Fracture direction with punch speed of (a) 30 mm/min^{-1}, optimum BHF and initial blank with a diameter of 80 mm, (b) 3 mm/min^{-1}, high BHF and initial blank with a diameter of 80 mm, (c) 3 mm/min^{-1}, optimum BHF and initial blank with a diameter of 82 mm

thickness reduces in the wall and this reduction is severe in the arc portion caused rupture at the arc portion. As a result, increasing the strain in the arc portion enhances martensite volume fraction in this location. The volume fraction of martensite of 0.60 and 0.577 was detected through experimental and FE simulation method, respectively.

Fig. 10 depicts different fracture mode in the arc portion of the cup with various punch speed. As can be seen in this figure, fracture propagates vertically to the load direction with punch speed

[DOI: 10.22068/ijmse.16.3.32]

of 30 mm min^{-1}, while the propagation angle of the fracture is tilted 45° to the force direction with punch speed of 3 mm min^{-1}, which is the preferred punch speed in this work. Based on Schmid's law, the yield stress of the material under plastic deformation is defined as the Eq. 4:

$$\sigma_y=\tau_{cr}/(\cos\lambda.\cos\varphi) \quad \text{Eq. 4}$$

where, $\cos\lambda.\cos\varphi$, is Schmid factor and τ_{cr} is the critical shear stress, which is created.

Minimum stress for yielding the material under deformation process occurs when the Schmid factor, which is known as $\cos\lambda.\cos\varphi$, is at its maximum. The highest amount of Schmid factor is 0.5 when $\lambda=\varphi=45°$. It has been proved that martensite forms on the active slip system that is mostly oriented to the 45° of the load direction due to high Schmid factor [38, 39]. It was also shown that austenitic stainless steels exhibit higher and lower yield stress under high and low strain rates, respectively, while their ultimate tensile strength may remain constant. It means that the ultimate tensile strength of the steel type 304L is insensitive to the strain rate, but yield stress is sensitive to the strain rate [22, 30, 31]. According to Fig. 10, the direction of the fracture propagation is vertical to the load direction under high punch speed of, 30 mm min^{-1}, but it is tilted 45° to the load direction under low punch speed of, 3 mm min^{-1}, due to minimum yield stress of the material with maximum Schmid factor in the case of $\lambda=\varphi=45°$.

4. CONCLUSION

In this paper, deep draw-ability of austenitic stainless steel type 304L was studied. Results of this study showed that LDR equal to 2 was obtained under optimum BHF of 1600 kgf at room temperature. The higher induced martensite volume fraction of 0.51 through experimental measurement and FE simulation method were occurred in the flange portion of the deep-drawn cup due to higher strain and stress concentration in this region. Rupture happened in the arc portion of the cup wall for blank with higher diameter. Also, higher amounts of induced martensite of 0.60 and 0.577 were transformed in the rupture location via experimental measurement and simulation method, respectively, because of higher strain and strain hardening in this region. Thickness distribution of the cup in FE simulation showed that thickness increases from bottom to the flange portion of the cup. Experimental procedures were simulated by LS-DYNA and the experimental results were in good agreement with the FE simulation.

REFERENCES

1. Lixin, L., Sheng, L., Ben, Y., Shengde, H. and Zhifeng, Z., "Quantitative Analysis of Strength and Plasticity of a 304 Stainless Steel Based on the Stress-strain Curve, Met. Mater." Int., 2016, 22, 391-396.
2. Wang, Z., Palmer, T. A. and Beese, A. M., "Effect of processing parameters on microstructure and tensile properties of austenitic stainless steel 304L made by directed energy deposition additive manufacturing, Acta." Materialia., 2016, 110, 226-235.
3. Jingwei, Z., Zhengyi, J., Guoqing, Z., Wei, D., Xin, Z. and Zhang, L., "Flow Behaviour and Constitutive Modelling of a Ferritic Stainless Steel at Elevated Temperatures, Met. Mater." Int., 2016, 22, 474-487.
4. Dutta, K., Kishor, R., Sahu, L. and Mondal, A. K., "On the role of dislocation characters influencing ratcheting deformation of austenitic stainless steel, Mater." Sci. Eng. A., 2016, 660, 47-51.
5. Buffa, G., Joining Ti6Al4V and AISI 304 through friction stir welding of lap joints: experimental and numerical analysis, Int." J. Mater. Form., 2016, 9 , 1, 59–70.
6. Wang, H., Jeong, Y., Clausen, B,. Liua, Y., McCabe, R. J., Barlatc, F. and Tome, N., "Effect of martensitic phase transformation on the behavior of 304 austenitic stainless steel under tension, Mater." Sci. Eng. A., 2016, 649, 174-183.
7. Halkaci, H. S., Turkoz, M. and Dilmec, M., "Enhancing formability in hydromechanical deep drawing process adding a shallow drawbead to the blank holder, J. Mater." Process. Technol., 2014, 214, 1638-1646.
8. Oujebbour, F. Z., Habbal, A., Ellaia, R. and Zhao, Z., "Multi criteria shape design of a sheet contour in stamping, J. Comput." Des. Eng., 2014, 1, 187-193.
9. Zein, H., Sherbiny, M. E., Abd-Rabou, M. and Shazly, M. E., "Thinning and spring-back prediction of sheet metal in the deep drawing process, Mater." Des., 2014, 53, 797-808.

[DOI: 10.22068/ijmse.16.3.32]

10. Behrens, G., Trier, F. O., Tetzel, H. and Vollertsen, F., "Influence of tool geometry variations on the limiting drawing ratio in micro deep drawing, Int." J. Mater. Form., 2014, 9, 2, 253–258.
11. Afshin, E. and Kadkhodayan, M., "An experimental investigation into the warm deep-drawing process on laminated sheets under various grain sizes, Mater." Des., 2015, 87, 25-35.
12. Dehghani, F. and Salimi, M., "Analytical and experimental analysis of the formability of copper-stainless-steel 304L clad metal sheets in deep drawing, Int." J. Adv. Manuf. Technol., 2016, 82, 163-177.
13. Zareh, D. B., Abaszadeh, Y. M. and Khalilpourazary, S., "The Effect of Nanoparticle Additives on Lubrication Performance in Deep Drawing Process: Evaluation of Forming Load, Friction Coefficient and Surface Quality, Int." j. précis. Eng. Manuf., 2015, 16, 5, 929-936.
14. Neto, D. M., Oliveira, M. C., Alves, J. L. and Menezeset, L. F., "Influence of the plastic anisotropy modelling in the reverse deep drawing process simulation, Mater." Des., 2014, 60, 368-379.
15. Wu, J. and Zou, F., "Deep Drawing Failure Map of a Coated Metal Sheet Based on the Process Parameters", J. Fail. Anal. Preven., 2016, 16, 361-368.
16. Anarestani, S. S., Morovvati, M. R. and Vaghasloo, Y. A., "Influence of anisotropy and lubrication on wrinkling of circular plates using bifurcation theory, Int." J. Mater. Form., 2015, 8, 439-454.
17. Quilliec, G. L., Raghavan, B. and Breitkop, P., "A manifold learning-based reduced order model for springback shape characterization and optimization in sheet metal forming, Comput. Methods." Appl. Mech. Eng., 2015, 285, 621-638.
18. Morovvati, M. R., Fatemi, A. and Sadighi, M., "Experimental and finite element investigation on wrinkling of circular single layer and two-layer sheet metals in deep drawing process, Int". J. Adv. Manuf. Technol., 2011, 54, 113-121.
19. Si-ji, Q., Bai-qing, X., Hong, L. and Zhang, T., "Critical blank-holder force in axisymmetric deep drawing, Trans". Nonferrous. Met. Soc. China., 2012, 22, 239-246.
20. Agrawal, A., Reddy, N. V. and Dixit, P. M., "Determination of optimum process parameters for wrinkle free products in deep drawing process, J. Mater". Process. Technol., 2007, 191, 51-54.
21. Beese, A. and Mohr, M. D., "Effect of stress triaxiality and Lode angle on the kinetics of strain-induced austenite-to-martensite transformation, Acta". Materialia., 2011, 59, 2589-2600.
22. Fathi, H., Emadoddin, E., Mohammadian Semnani, H. R. and Mohammad Sadeghi, B., "Effect of Punch Speed on the Formability Behavior of Austenitic Stainless Steel Type 304L, Met". Mater. Int., 2016, 22, 397-406.
23. Yeddu, H. K., Lookman, T. and Saxena, "A., Strain-induced martensitic transformation in stainless steels: A three-dimensional phase-field study, Acta". Materialia., 2013, 61, 6972-6982.
24. Dilmec, M. and Arap, M., "Effect of geometrical and process parameters on coefficient of friction in deep drawing process at the flange and the radius regions, Int". J. Adv. Manuf. Technol., 2016, 86, 1-13.
25. Karajibani, E., Fazli, A. and Hashemi, R., "Numerical and experimental study of formability in deep drawing of two-layer metallic sheets, Int". J. Adv. Manuf. Technol., 2015, 80, 113-121.
26. Hausild, P., Kolarik, K. and Karlik, M., "Characterization of strain-induced martensitic transformation in A301 stainless steel by Barkhausen noise measurement, Mater". Des., 2013, 44, 548-554.
27. Fathi, H., Emadoddin, E. and Mohammadian Semnani, H. R., "Simulation and experimental investigation of strain rate impact on martensitic transformation in 304L steel through dome test, J. Mater." Res., 2016, 31, 2136-2146.
28. Masumura, T., Nakada, N., Tsuchiyama, T., Takaki, S., Koyano, T. and Adachi, K., "The difference in thermal and mechanical stabilities of austenite between carbon- and nitrogen-added metastable austenitic stainless steels, Acta". Materialia., 2015, 84, 330-338.
29. LS-DYNA Keyword User's Manual Version 971, "Livermore software technology corporation", USA, 2007, 1, 424-428.
30. Das, A. and Tarafder, S., "Experimental investigation on martensitic transformation and fracture morphologies of austenitic stainless steel, Int". J. Plast., 2009, 25, 2222-2247.
31. Lo, K. H., Zeng, D. and Kwok, C. T., "Effects of sensitisation-induced martensitic transformation on the tensile behaviour of 304 austenitic stainless steel, Mater". Sci. Eng. A., 2011, 528, 1003-1007.
32. Mohammad Sadeghi, B., "analyse et identification du comportement mécanique aciers à effet TRIP à partir de mesure de champs cinematiques, in Laboratoire de Physique et Mécanique des Matériaux, Ph.D thesis, Metz". Paris. Tech., 2011, 24-27.
33. Jayahari, L., Balunaik, B., Gupta, A. K. and KumarSingh, S., "Finite element Simulation studies of AISI 304 for deep drawing at various temperatures, Mater". Today. Proceedings., 2015, 2, 1978-1986.

[DOI: 10.22068/ijmse.16.3.32]

34. Lebedev, A. A. and Kosarchuk V. V., "Infuence of phase transformations on the mechanical properties of austenitic stainless steels, Int". J. Plast., 2000, 16, 749-767.
35. Tourki, Z., Bargui, H. and Sidhom, H., "The kinetic of induced martensitic formation and its effect on forming limit curves in the AISI 304 stainless steel, J. Mater". Process. Technol., 2005, 166, 330-336.
36. Stringfellow, R. G., Parks, D. M. and Olson, G. B., "A constitutive model for transformation plasticity accompanying strain-induced martensitic transformations in metastable austenitic steels, Acta". Metall. Mater., 1997, 40, 1703-1716.
37. Li, N., Wang, Y. D., Liu, W. J., An, Z. N., Liu, J. P., Su, R., Li, J. and Liaw, P. K., "In situ X-ray microdiffraction study of deformation-induced phase transformation in 304 austenitic stainless steel, Acta". Materialia., 2014, 64, 12-23.
38. Bollenhagen, C. M., Zimmermann, M. and Christ, H. J., "Very high cycle fatigue behaviour of austenitic stainless steel and the effect of strain-induced martensite", Int, J, Fatigue,, 2010, 32, 936-942.
39. Barnettm M. R,, Ghaderi, A. and Fonseca, J. Q., Robson J D, "Influence of orientation on twin nucleation and growth at low strains in a magnesium alloy, Acta". Materialia., 2014, 80, 380-391.

[DOI: 10.22068/ijmse.16.3.32]